Stability and reproducibility of co-electrospun brain-mimicking phantoms for quality assurance of diffusion MRI sequences

Accepted Manuscript

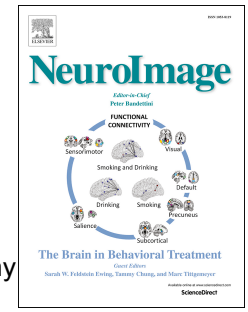

Stability and reproducibility of co-electrospun brain-mimicking phantoms for quality assurance of diffusion MRI sequences

Matthew Grech-Sollars, Feng-Lei Zhou, Adam D. Waldman, Geoff J.M. Parker, Penny L. Hubbard Cristinacce

PII: S1053-8119(18)30566-4

DOI: 10.1016/j.neuroimage.2018.06.059

Reference: YNIMG 15065

To appear in: *NeuroImage*

Received Date: 28 February 2018

Revised Date: 23 May 2018

Accepted Date: 20 June 2018

Please cite this article as: Grech-Sollars, M., Zhou, F.-L., Waldman, A.D., Parker, G.J.M., Hubbard Cristinacce, P.L., Stability and reproducibility of co-electrospun brain-mimicking phantoms for quality assurance of diffusion MRI sequences, *NeuroImage* (2018), doi: 10.1016/j.neuroimage.2018.06.059.

Stability and reproducibility of co-electrospun brain-mimicking phantoms for quality assurance of diffusion MRI sequences

Matthew Grech-Sollars[1,2]*, Feng-Lei Zhou[3*], Adam D Waldman[4,5], Geoff J. M. Parker[2,6], Penny L. Hubbard Cristinacce[3]
[1]*Department of Surgery and Cancer, Imperial College London;*
[2]*Department of Imaging, Imperial College Healthcare NHS Trust;*
[3]*Centre for Imaging Sciences, The University of Manchester;*
[4]*Centre for Clinical Brain Sciences, The University of Edinburgh, Edinburgh;*
[5]*Department of Medicine, Imperial College London*
[6]*Bioxydyn Limited, Manchester.*

**Joint first author*
m.grech-sollars@imperial.ac.uk; fenglei.zhou@manchester.ac.uk

Abstract
Grey and white matter mimicking phantoms are important for assessing variations in diffusion MR measures at a single time point and over an extended period of time. This work investigates the stability of brain-mimicking microfibre phantoms and reproducibility of their MR derived diffusion parameters. The microfibres were produced by co-electrospinning and characterized by scanning electron microscopy (SEM). Grey matter and white matter phantoms were constructed from random and aligned microfibres, respectively. MR data were acquired from these phantoms over a period of 33 months. SEM images revealed that only small changes in fibre microstructure occurred over 30 months. The coefficient of variation in MR measurements across all time-points was between 1.6% and 3.4% for MD across all phantoms and FA in white matter phantoms. This was within the limits expected for intra-scanner variability, thereby confirming phantom stability over 33 months. These specialised diffusion phantoms may be used in a clinical environment for intra and inter-site quality assurance purposes, and for validation of quantitative diffusion biomarkers.

Highlights

- Grey and white matter mimicking phantoms showed mean diffusivity and fractional anisotropy values typical of tissue.
- Diffusion measures for the phantoms were stable over 33 months.
- The porosity of the phantoms was observed to be stable over 30 months.
- The phantoms may be used for QA purposes in a clinical environment and for validation of quantitative diffusion biomarkers.

Keywords
Diffusion MRI, brain phantom, hollow microfibers, co-electrospinning, white matter phantom, gray matter phantom

1 Introduction

The routine use of diffusion MRI sequences in the clinic, and of more advanced diffusion sequences in a research environment, have led to a need for developing specialist phantoms with known geometry and microstructural characteristics for quality assurance purposes (Barnes et al., 2017). The importance of such specialist phantoms lies in analysing the variability of acquired data from different scanners (particularly for multi-centre studies), in assessing the long-term stability of scanners (particularly for longitudinal studies and clinical quantitative imaging) and in providing a ground truth for methods designed to provide quantitative measures of tissue microstructure. Phantoms should therefore be able to reproduce the physical properties of the tissue they are intended to mimic as well as be stable over an extended period of time.

In the case of diffusion brain imaging the phantom should mimic grey and white matter structures in terms of both diffusivity and anisotropy. Recent studies have reported a novel type of brain and cardiac phantom designed from electrospun hollow polycaprolactone (PCL) hollow microfibers infused with cyclohexane. These phantoms demonstrated suitable tissue-mimicking properties and were successfully used for the validation of diffusion MRI (Hubbard et al., 2015; Teh et al., 2016; Ye et al., 2014; Zhou et al., 2015, 2012). Moreover, the short-term (up to 4 months) stability and reproducibility of PCL/cyclohexane phantoms was also shown (Teh et al., 2016; Zhou et al., 2012). In particular, the microstructure of co-electrospun PCL fibres remained visibly intact in cyclohexane over a period of 1 week (Zhou et al., 2012) and the coefficient of variation (CV) for the apparent diffusion coefficient (ADC) and FA of a cardiac-mimicking PCL fibres phantom filled with cyclohexane were found to be 2.07% and 1.67% over the 4 month period (Teh et al., 2016).

However, hydrolysis of the PCL polymer is known to occur when immersed in phosphate buffered saline at 37°C over a period of three months (Bosworth and Downes, 2010). While the degradation of PCL has been studied *in vitro* and *in vivo* (Woodruff and Hutmacher, 2010), previous work reporting PCL degradation in cyclohexane is scarce, which is of importance to the developed cyclohexane-filled PCL-based phantoms. This paper evaluates the stability of cyclohexane-filled PCL phantoms as brain-mimicking structures using scanning electron microscopy (SEM) over 30 months and diffusion MRI measurement reproducibility over 33 months.

2 Material and Methods

2.1 Phantom Construction

Fibre phantoms were constructed using co-electrospinning (co-ES) on a lab-scale setup (Fig. 1), details described in a previous study (Zhou et al., 2011). Aligned and random hollow PCL

microfibres were produced in the co-ES processes to respectively mimic the diffusion MRI properties of brain white matter and grey matter, using a rotating mandrel with 800 rpm and a static collector. A previous study reported that the cross-sectional microstructures generated can be influenced by production time, solution flow rate and *x-y* stage translation speed (Zhou et al., 2015, 2012). Here aligned fibres with small and large inner diameters were produced using the core flow rates of 0.8 ml/h and 2.0 ml/h, respectively.

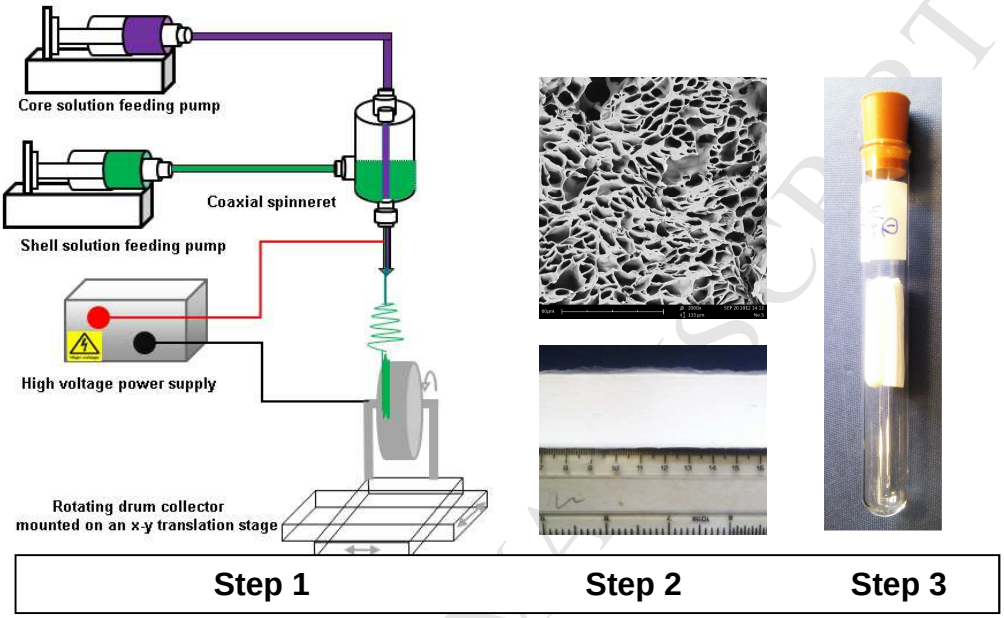

Fig. 1. Schematic of coaxial electrospinning of hollow polymeric microfiber phantom. Step 1: Co-electrospinning of aligned hollow microfibres; Step 2: A fibre strip (bottom) and SEM micrograph showing fibre cross section (top); Step 3: MR phantom constructed from fibre strip layers.

Two aligned fibre strips with large and small inner diameters were prepared using 0.8 and 2.0 mL/h core flow rates while the shell flow rate was kept at 3 mL/h, applied voltage at 9.0 kV, and working distance between the coaxial spinneret and the fibre collector at 5 cm. The fibre sample produced at 0.8 mL/h core flow rate was used for the white matter mimicking phantom WM1, and the 2.0 mL/h core flow rate for WM2. Two small white matter material samples were manufactured for assessing the structural stability on SEM and two larger white matter material samples were manufactured for assessing the stability of MRI diffusion parameters.

In order to create the grey matter mimicking phantoms, different process parameters were used to generate randomly oriented fibres that were only formed in a sufficient long working distance where whipping instability occurred to the fluid jet in electrospinning (Zhou et al., 2011). Two random fibre meshes with large and small inner diameters were prepared using the following settings: 10.0 kV or 20.0 kV applied voltage, 0.8 or 0.2 mL/h core flow rate, 20 cm working distance and 3.0 ml/h shell flow rate. The grey matter-mimicking phantom GM1 was created using a 10 kV applied voltage and a 0.8m L/h flow

core rate and GM2 using a 20 kV applied voltage and a 0.2 mL/h core flow rate. In this case, only two large phantoms for assessing the stability of diffusion MRI parameters were manufactured. It was assumed that the structural stability of grey matter phantoms would be the same as that of the white matter phantoms and hence no small samples were manufactured for SEM assessment.

Based on the method described previously (Hubbard et al., 2015), each of the large white and grey matter phantoms created for assessing diffusion MRI parameters consisted of a number of co-electrospun fibre layers packed into glass tubes (20 mm outer diameter), filled with cyclohexane and with a PTFE barrier position behind the phantom at the far end of the tube to keep air bubbles away from the imaging volume. The four tubes were kept in an airtight container and stored upright.

2.2 SEM characterization of co-ES fibres

Co-ES fibres were characterised using SEM combined with a freeze fracture technique. The fibres were immersed in a liquid nitrogen bath for about 20 min until the sample was completely frozen. Sharp scissors were then cooled in the bath and used to quickly cut the fibres in one step. The cross-sections of co-ES fibres (0.5-1mm thickness) were observed using a Phenom G2 pro desktop SEM (Phenom-World). SEM images were acquired at 7 time points: 0, 1, 3, 6, 12, 24 and 30 months for the white matter phantoms created for structural assessment, and at 2 time points, 0 and 25 months for one of the grey matter phantoms (GM2) created for MRI assessment. Three SEM images were acquired from different locations within the phantoms at each time point to assess their porous structures and the average measurement of the three images was reported. A small number of very large pores (up to 1 % of total measurements) were masked to avoid the introduction of outliers in the measurements. Area-averaged and number-averaged methods were used to calculate the intra- and inter-fibre pore sizes of co-ES fibre assemblies (Zhou et al., 2015). Considering the wide range of pore sizes (from submicron to about 10 µm or larger), the area-averaged method was found to be more appropriate to evaluate the pore size change caused by process parameters such as the core flow rate (Hubbard et al., 2015).

The cross-sectional area-weighted average pore size and porosity were calculated by converting an SEM image to a binary image and thresholding using a previously reported ImageJ based method (Zhou et al., 2015). These are defined by:

$$\text{area-weighted average pore size} = \frac{\sum D_i A_i}{\sum A_i}$$

$$\text{area-weighted porosity} = \frac{\sum A_i}{A} \times 100\%$$

where D_i is the diameter of the ith pore, A_i is the area of the ith pore, and A is the total area of the measured image.

2.3 MR Image Acquisition and Analyses

The phantoms were imaged on a clinical Siemens Avanto 1.5 T system during 4 sessions: once at 0 months, twice at 0.5 months, twice at 17 months and twice at 33 months. Over this time period the phantoms were left immersed in cyclohexane and stored vertically. Occasional refilling of cyclohexane in the phantom tubes was necessary during this time period due to evaporation. Phantoms were visually checked for air bubbles prior to scanning. The first MRI scan (0 months) took place one month after the phantom was created and immersed in cyclohexane. The phantoms were placed vertically in the scanner so as to avoid the risk of cyclohexane spilling out of the tubes. They were also left in the scanner room for an hour before scanning to reach room temperature. Phantoms were visually checked for air bubbles prior to scanning. The protocol included a standard PGSE DTI sequence with a 2 mm isotropic voxel size, 30 gradient directions distributed over a whole sphere (b = 0, 1000 s/mm^2), TR = 11000ms, TE = 88ms, FOV of 240 mm x 240 mm and using a 12-channel head coil.

DTI data was eddy-corrected (using "eddy_correct") and processed using FSL v5.0.9 (Jenkinson et al., 2012) to extract the fractional anisotropy (FA) and mean diffusivity (MD) maps. Regions of interest (ROIs) were drawn in FSLview around each of the phantoms across each time point and the mean and standard deviation for each parameter were calculated. The coefficient of variation across the whole dataset for each phantom was measured for MD and FA as the standard deviation for the averaged parameter values over all scans divided by the global average.

3 Results

3.1 Structural stability of hollow PCL fibres

Cross sections of the two WM phantoms examined by SEM (Fig. 2 and Fig. 3) reveal that small and large fibres remain porous across 30 months period in cyclohexane. The two dominant characteristic structural features are pores and merging fibres. The wall of small fibres at the time point of 12 months (Fig. 2) appear thicker and look apparently different from those at other time points.

Analysis of the SEM images revealed that there were some changes in the pore size and porosity of co-ES fibres over a period of 30 months. Pore diameter distribution, area-weighted average pore size and porosity of the two fibre types at 7 time points are shown in Fig. 4. The pore diameter distributions in the two white matter phantoms (0.8ml/h and 2.0ml/h) had a wide range from submicron to ten microns (Fig. 4a and b), and could not be compared. The area-weighted pore diameter was therefore used to compare phantoms. The original area-weighted average pore size of WM1 (core flow rate 0.8 ml/h, averaged over three locations) was 6.8 µm and varied between 89% and 103% of the original value over the 30-month period (min 6.1 µm at 12 months; max 7.0 µm at 6 months; mean 6.6µm); while the original area-weighted average pore size of WM2 (core flow rate 2.0 ml/h) was 8.3 µm and varied between 88% and 110% of the original value over the 30-month

period (min 7.3 µm at 24 months; max 9.2 µm at 1 month; mean 8.2 µm) (Fig. 4a). Fig. 4b demonstrates the corresponding porosity (averaged over three locations), starting at 63.8% and then varying between 43.6% (12 months) and 55.4% (1 month) for WM1; and starting at 67.7% and then varying between 44.1% (12 months) and 53.6% (3 months) for WM2 over 30 months. The coefficient of variation (CV) for the pore size was 5.1% and 6.9% in WM1 and WM2 respectively. The CV for the porosity was 10.2% and 13.4% in WM1 and WM2 respectively. SEM images of the cross section of GM1 phantom are shown in Fig. 5. The images show the random orientation of fibres both at 0 months and after 25 months of immersion in cyclohexane.

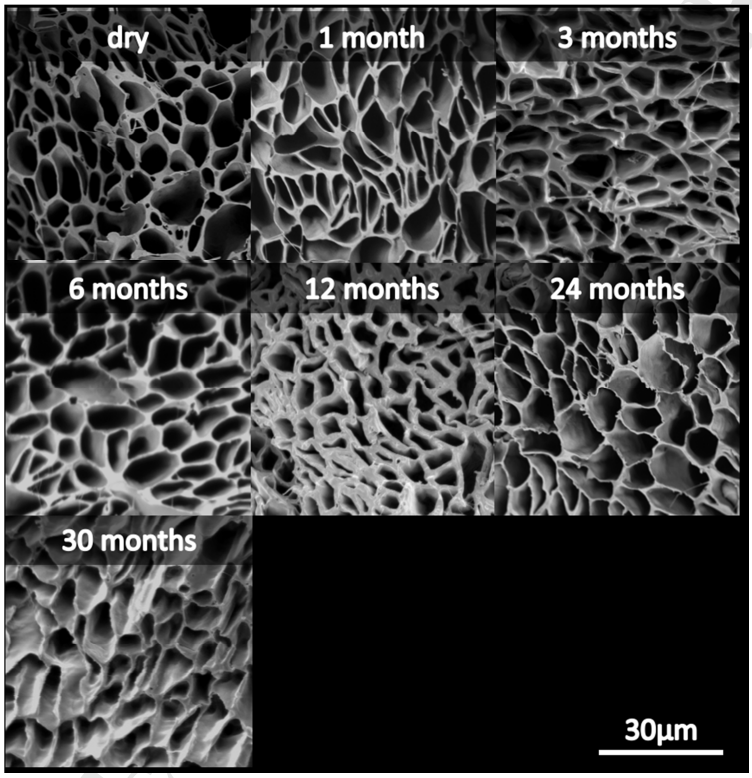

Fig. 2. SEM images of 0.8 ml/h aligned fibres (WM1) at "dry" (before immersion inside cyclohexane) and at 1, 3, 6, 12, 24 and 30 months after immersed in cyclohexane. The fibre walls at month 12 appeared thicker than at the other time points. SEM images at each time point were acquired from different regions of the phantoms.

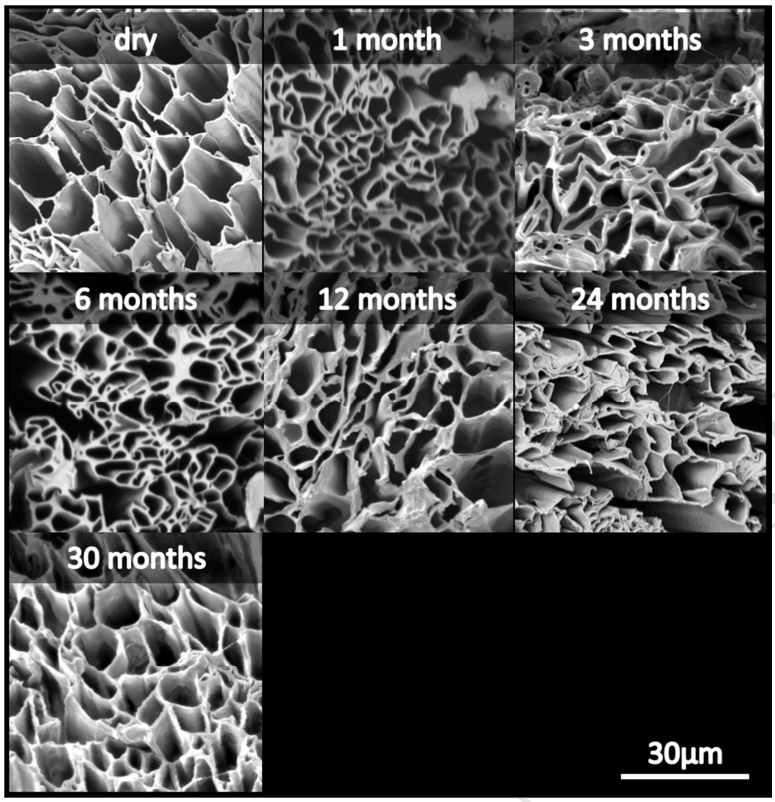

Fig. 3. SEM images of 2.0 ml/h aligned fibres (WM2) at "dry" (before immersion inside cyclohexane) and at 1, 3, 6, 12, 24 and 30 months after immersed in cyclohexane. SEM images at each time point were acquired from different regions of the phantoms.

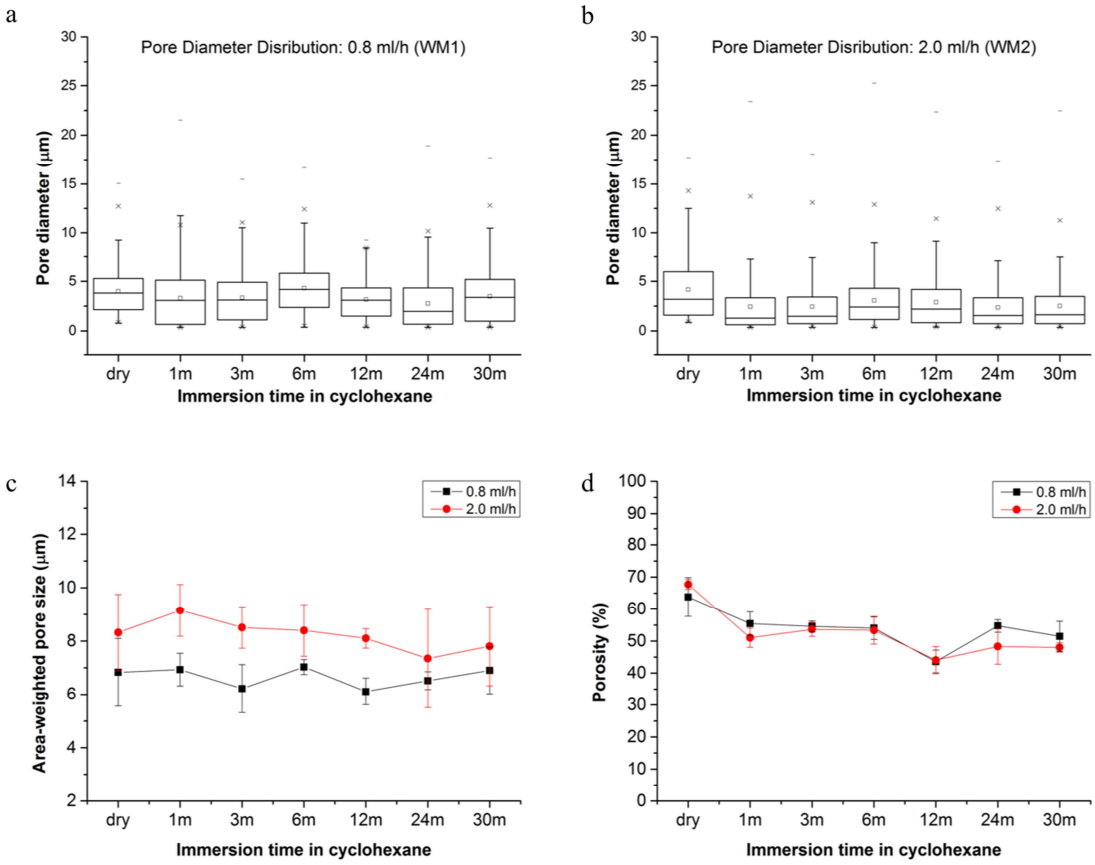

Fig. 4. Pore diameter distribution of (a) 0.8 ml/h (WM1) and (b) 2.0 ml/h aligned fibres (WM2) over the 30-month period. The 1 and 99 percentiles are marked with an "X" while the min and max are shown using "_". (c) Area-weighted average pore size and (d) porosity over 30 months of small and large fibres produced at both 0.8 ml/h and 2.0 ml/h.

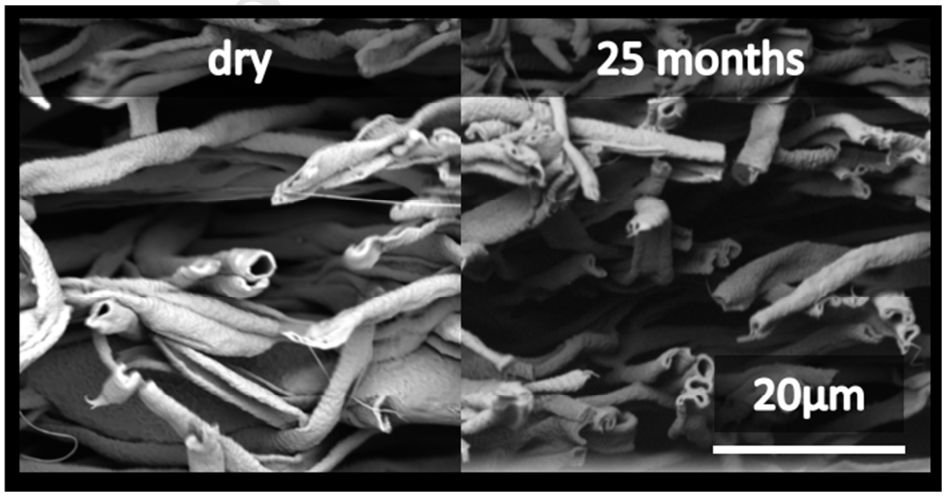

Fig. 5 SEM images from GM2 show porous random cross section of the GM fibres when dry at "dry" (before immersion inside cyclohexane) and after being immersed in cyclohexane for 25 months. SEM images at each time point were acquired from different regions of the phantoms.

3.2 MRI parameter reproducibility

The mean and standard deviation values for each of the phantoms over the whole time period are shown in Fig. 6. The average FA and MD over time was within one standard deviation of the average value at any single session for all phantoms except for MD in GM2 at the first scan of month 33. Results for the variability in MD and FA are shown in Table 1. Excluding FA in the grey matter phantoms, which is not normally measured clinically, the coefficient of variation (CV) over both WM and GM phantoms in MD and FA varied between 1.6 and 3.4% (mean 2.6%). The CV for FA in the grey matter phantoms, where a high CV is expected due to the naturally low FA value, was of 8.9 and 18.7%.

Fig. 6. (a) DTI images showing FA (left and top right) and MD (lower right) in the 4 phantoms analysed. The colour in the FA image represents the

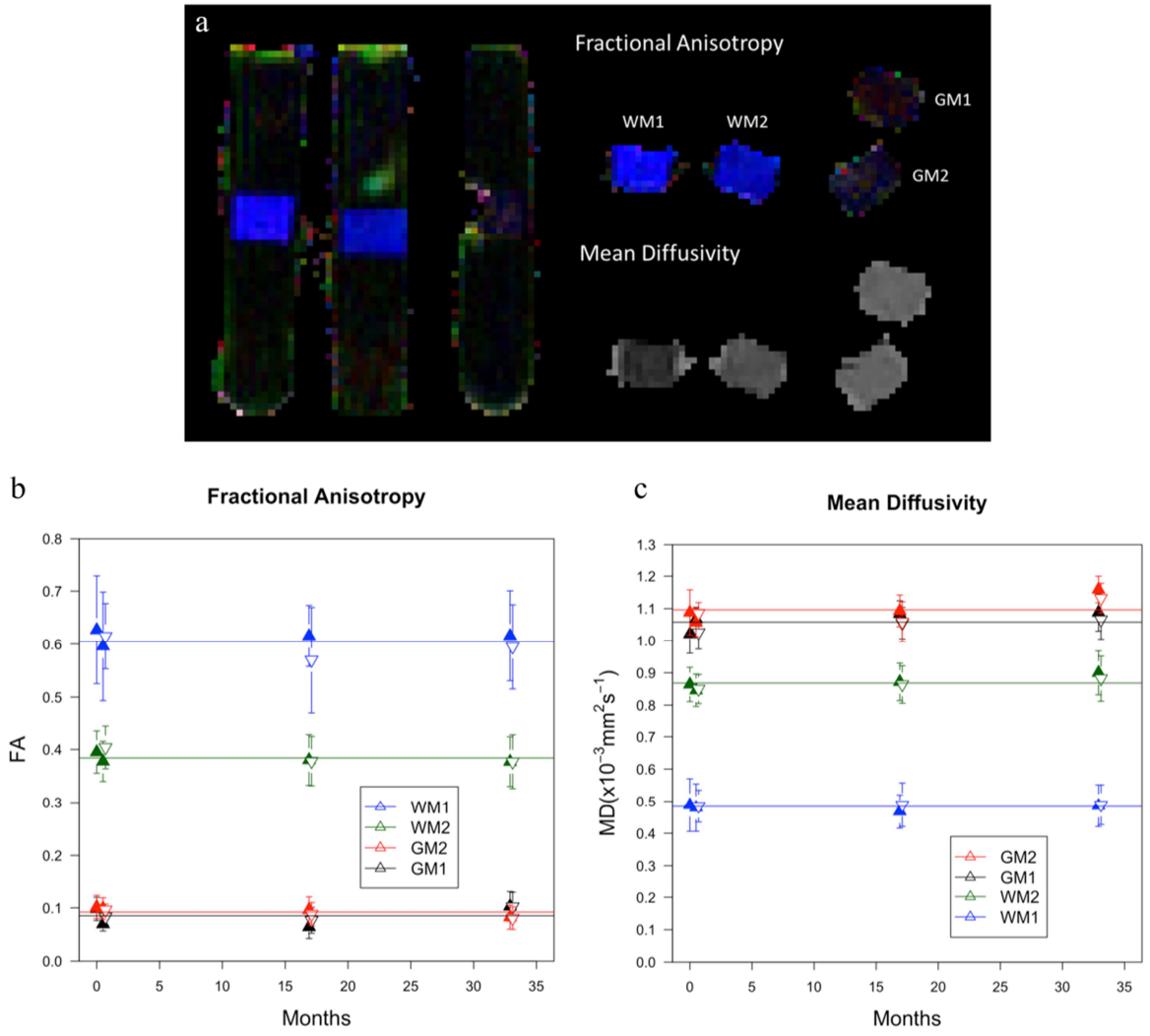

direction of the primary eigenvector (blue: up/down; red: left/right; green: through-plane). The WM phantoms have a higher FA with preferential diffusion in one direction (blue) and lower MD, while the GM phantoms have a low FA with diffusion in different directions and a higher MD. Stability measurements for MD and FA in the four phantoms are shown over a 33 month period in (b) and (c). The plots show the

mean and standard deviation measured at each time point. Coloured triangles indicate the first scan within a session while white triangles indicate a repeat scan within the same session. The mean value over time is also shown on the graphs (horizontal lines).

Table 1: Variability across all time-points for MD and FA in all phantoms. Individual values at each time-point are shown to three decimal places. With μ=mean, σ=standard deviation, CV= coefficient of variation

	MD ($x10^{-3}$ mm^2s^{-1})				FA			
	WM1	WM2	GM1	GM2	WM1	WM2	GM1	GM2
Month 0	0.488	0.864	1.021	1.088	0.627	0.395	0.098	0.102
Month 0.5 (1)	0.480	0.846	1.068	1.057	0.596	0.378	0.070	0.099
Month 0.5 (2)	0.485	0.85	1.026	1.086	0.615	0.404	0.083	0.096
Month 17 (1)	0.468	0.872	1.084	1.093	0.615	0.390	0.064	0.096
Month 17 (2)	0.489	0.864	1.055	1.059	0.570	0.378	0.077	0.088
Month 33 (1)	0.486	0.900	1.088	1.159	0.616	0.377	0.103	0.083
Month 33(2)	0.489	0.882	1.066	1.132	0.595	0.377	0.103	0.081
μ	0.484	0.868	1.058	1.096	0.605	0.384	0.085	0.092
σ	0.0076	0.0186	0.0263	0.0373	0.0193	0.0108	0.0159	0.0082
CV (%)	1.6	2.1	2.5	3.4	3.2	2.8	18.7	8.9

4 Discussion

Diffusion MR imaging is widely used in multi-centre studies, which introduces the question of whether data obtained using clinical sequences on different scanners with different field strengths are comparable. This question also arises in longitudinal studies, where patients may be imaged on the same or different scanners at various time-points and the variability in the diffusion measurements over time needs to be assessed, particularly following a significant MRI system upgrade.

4.1 Acceptable reproducibility

A value of reproducibility for a quantitative measurement is acceptable if it is lower than the effect size that it is trying to measure. The stability of the phantom needs to be assessed in light of the expected variability which would be observed for FA and MD values when imaging twice on the same MR system. A recent study assessed reproducibility of diffusion measurements on eight scanners (4 Siemens 1.5 T, 4 Philips 3.0 T) using an ice-water phantom and healthy volunteers across five institutions (Grech-Sollars et al., 2015). That study showed the intra-scanner reproducibility for MD in grey and white matter and FA in white matter to be 2.5% or less, whereas the CV for FA in grey matter was higher at 7.4% due to the low values of FA being impacted more by noise. We assess the longitudinal reproducibility of the phantoms in view of these differences which are expected when scanning the same person twice on the same scanner.

MR results for the phantoms (Fig. 6) showed a CV between 1.6 and 3.4% (mean 2.4%) for MD across all phantoms and for FA in the WM phantoms (Table 1), comparable to the variability expected in repeat scans within the same session as previously reported (Grech-Sollars et al., 2015). The CV for FA in grey matter phantoms was higher (8.9% in one phantom and 18.7% in the other), as expected in media with a naturally low value of FA (Grech-Sollars et al., 2015).

4.2 Variability in phantom manufacture

A previous study on five PCL phantoms created using a 0.8 ml/h flow rate on a 3 T clinical scanner found that the coefficient of variation for FA between the five phantoms was 3.4% as reported in the supplementary information (Hubbard et al., 2015). That reproducibility shows the variation which exists from producing more than one phantom and includes in it the intra-scanner variability (scan-rescan repeatability). The CV measured across different phantoms was in line with the reproducibility measured here in a single phantom produced using the same flow rate over a period of 33 months (3.2%). As the variability is comparable to expected intra-scanner variations, it is possible that little is changing in the phantoms over time.

4.3 Physical phantoms vs PCL vs PP phantoms

Physical phantoms that mimic brain white matter are often made from glass or plastic capillary and textile filament fibres. However, to date these fibre phantoms have shown dissimilarity between their microscopic geometry and the characteristics of real tissue. Many of these fibres are either not hollow, impermeable, or they have an inner and/or outer diameter far outside the range of neuronal white matter fibres. In previous studies (Anderson et al., 2011a, 2011b; Gates and Cameront, 1998) hollow fibre MR phantoms were made of commercial fibre modules (dialyzer and bioreactors) with inner diameters of typically 200−300 µm, which is much larger than axon fibre size of 0.1−10 µm. More recently, melt-spun hollow polypropylene (PP) microfibres were also used to construct brain white matter phantoms (Fan et al., 2018; Guise et al., 2016).

Co-electrospun PCL microfibres have a variable and tuneable range of sizes similar to those in brain or cardiac tissues, but require longer operational time to prepare thicker samples. In contrast, fibres in melt-spun PP phantoms have less variable sizes and thicker walls, but can be produced in shorter operational time. The yield of co-electrospun hollow microfibres can be enhanced by novel spinnerets (Labbaf et al., 2014; Lucie et al., 2014; Yan et al., 2015). In addition, melt spinning of hollow PP microfibres usually requires strict process control and a complex and expensive spinneret that has to be specially designed (De Rovere, 2000; Guise et al., 2016). PP fibres are hydrophobic and therefore phantoms made from these fibres require pressure filling with water, which could be improved by adding hydrophilic amphiphilic surfactants (Liang et al., 2016). Our most recent study has demonstrated the presence of the polysiloxane-based surfactant in the PCL fibres can alter the hydrophobicity of the resultant phantom (Zhou et al., 2018).

The mean diffusivity measured from both cyclohexane-filled PCL phantom and water-filled PP phantom is within the range of the brain's white matter; co-electrospun PCL fibres with various sizes can lead to a change in the diffusion signal (Hubbard et al., 2015). PCL fibres and PP fibres can be further constructed into complex phantoms with various crossing angles (Guise et al., 2016; Hubbard et al., 2014), which results in the change in MR measurements, especially for higher angles, e.g., 45° and 90°. Co-electrospun fibres were also used to make a cardiac diffusion phantom comprising three layers of fibres wound at different helix angles, from which DTI confirms the fibre tracks in the phantom (Teh et al., 2016). In addition, co-electrospun materials can be tuned into hollow microspheres employed to construct tumour cell mimicking phantoms (Mchugh et al., 2017; McHugh et al., 2015).

The design of physical phantoms requires appropriate chemical stability and reproducibility. It is important that the material does not degrade or change structure within a reasonable time window. PP filaments exposed to a saline solution showed a loss of material to the solution and a decrease of about 10 % in diameter over the period of 30 days (Silva et al., 2007). PP fibres possess low degradability especially in water when compared to PCL, which could improve PP phantom durability (Arutchelvi et al., 2008; Guise et al., 2016). PCL was chosen partly due to its relatively high fibre formability and process stability compared with other electrospinnable polymers (Woodruff and Hutmacher, 2010).

4.4 Pore size and porosity

The hollow centre of the fibres and the spaces between fibres when closely packed appear as pores in SEM cross-sections; these pores can be classified into intrafibre pores, interfibre pores and void pores, each of which has distinct features (Zhou et al., 2015). Among these pores, only intrafibre pores are controllable by co-ES parameters. A large number of outliers and extremes were observed during the freeze fracture sampling process, indicating that void pores were present in most of aligned fibre samples, which contributes to the variability between immersion time points. We therefore excluded the very large pores (up to 1% of total measurements) to reduce the effect of these outliers on our measurements. The porous microstructures of WM1 and WM2 were observed to be stable over 30 months, particularly after the 1st month of immersion in cyclohexane. GM2 was also observed to be porous after 25 months immersion in cyclohexane.

4.5 Fibre wall thickness

In theory, it can be envisaged that thicker walls could slow down the penetration of the diffusion liquid (cyclohexane) into the hollow PCL fibres. For grey matter fibre phantoms having similar inner diameters, packing density (number of fibres/unit area) and fibre walls that are well defined (Fig 5), thicker walls may reduce the extra-fibre space, which we would expect to result in a decrease in ADC but not FA, due to the lack of fibre alignment in these samples. In the white matter phantoms, the merged nature of the fibres means that the

extra-fibre space is not clearly defined, making the impact of differences in fibre wall thickness hard to predict.

The fibre wall thickness at 12 months for WM1 was observed to be greater than at other time points (Fig. 2). It is unlikely that this is a result of immersion time in cyclohexane as such thicker walls are not present in later images. In addition, although the sectioning position at each time point was random and there is an element of variability in the pore structure at different positions of the phantom, we have not previously observed any major differences in fibre wall width. It may be that the reason for this increase in size at 12 months was the result of some cyclohexane remaining in the PCL fibres at a particular location before freezing and cutting of the sample, inducing some swelling in the fibre walls.

4.6 SEM and MR Imaging comparison

The significant difference in pore size between the two WM phantoms is responsible for the differences in MD and FA between WM1 and WM2. The phantom creation process is able to control the intrafibre pores, but not the interfibre and void pores. A phantom with a higher FA can be created by further increasing the orientation of fibres by increasing the speed of a rotating drum fibre collector in the co-electrospinning process shown in Fig 1. We would therefore expect MR to detect variations in pore size and porosity. However, the SEM showed higher coefficients of variation in pore size (5.1% - WM1 and 6.9% - WM2) and porosity (10.2% - WM1 and 13.4% - WM2) over 30 months, as compared to MD (1.6% - WM1 and 2.1% - WM2) and FA (3.2% -WM1 and 2.8% - WM2) measurements. SEM results showed that the main change in porosity happened within the first month after immersion into cyclohexane and appeared stable after that (Fig. 4d). Excluding the first time-point (dry) brought the CV for porosity to 8.5% in WM1 and 7.4% in WM2. The fact that our first MRI scan took place one month after immersion into cyclohexane may be the reason for not having captured this initial variation in structure. Furthermore, differences observed in the structural characteristics determined by SEM could be a result of a variety of factors, including the freeze fracture preparation method, the phantom region in which measurements are made, and polymer degradation. This means that variation of SEM measurements could be a result of the technique and sampling location rather than a real change over time in phantom structure. In order to minimise this effect, we took measurements from three different locations and averaged the measurements out. MR measurements are averaged over a much larger volume and are non-destructive – thereby allowing for repeat measurements in the same voxel. The difference in the two imaging techniques could therefore be another reason for not capturing the variations seen on SEM using MRI.

Longitudinal variations in MD and FA were within the limits expected for intra-scanner variability. The average value over time was within one standard deviation of the mean measure at any single time-point in all cases except for the MD in GM2 at 33 months. Of note, this phantom was removed from its containing tube at month 25 to be imaged on the

SEM, which may have altered the distribution of the fibres within the phantom and therefore the physical properties which the mean diffusivity represents. However, the second scan within that same session at 33 months was nonetheless within one standard deviation of the mean, thereby confirming the phantom stability over the 33 months.

4.7 Limitations and recommendations

A number of limitations exist both with respect to microstructural SEM measurements and diffusion MR measurements. Pore distortion resulting from the freeze fracture method produced inevitable errors with the calculated diameters and porosity. The semi-automated sampling and measurement process may have contributed to the variability observed with immersion time. With respect to MR measurements, as diffusion measures are affected by temperature, normal fluctuations in the temperature of the MR room may have contributed to some of the changes in diffusion values. In this study, the temperature was measured at two of the time-points inside the phantom box at the start and end of the acquisition and varied between 20 and 24°C. Moreover, SEM characterisation is a destructive method and hence we were unable to measure the microstructure of the same phantom on both SEM and MRI.

Further issues with the use of cyclohexane-filled PCL phantoms are that they require regular filling in a fume-cupboard, appropriate storage, and to be transported and handled with care. A hydrophilic water-based phantom would be more appropriate for use in a clinical environment and future work will focus on the development of such a phantom.

4.8 Conclusion

The longitudinal stability shown in this study validates the use of co-ES brain-mimicking phantoms in the development of diffusion MRI methods, as well as for routine quality assurance purposes and for establishing MRI system performance in multicentre trials. To our knowledge these are the first synthetic, controllable phantoms mimicking both white and grey matter microstructure for diffusion MRI.

Acknowledgements: MGS and FLZ contributed equally to this work. The authors would like to thank Lesley Honeyfield and Caroline Renaud at Imperial College Healthcare NHS Trust for their help in this study.

Funding: This work was supported by "CONNECT", the FET Programme (FET-Open grant number: 238292), The Brain Tumour Charity, the Brain Tumour Research Campaign, and the CRUK and ESPRC Cancer Imaging Centre in Cambridge and Manchester (C8742/A18097).

References

Anderson, J.R., Ackerman, J.J.H., Garbow, J.R., 2011a. Semipermeable hollow fiber phantoms for development and validation of perfusion-sensitive mr methods and signal models. Concepts Magn. Reson. Part B Magn. Reson. Eng. 39B, 149–158. https://doi.org/10.1002/cmr.b.20202

Anderson, J.R., Ye, Q., Neil, J.J., Ackerman, J.J.H., Garbow, J.R., 2011b. Diffusion effects on longitudinal relaxation in poorly mixed compartments. J. Magn. Reson. 211, 30–36. https://doi.org/10.1016/J.JMR.2011.03.018

Arutchelvi, J., Sudhakar, M., Arkatkar, A., Doble, M., Bhaduri, S., Uppara, P.V., 2008. Biodegradation of polyethylene and polypropylene. Indian J. Biotechnol. 7, 9–22.

Barnes, A., Coutts, G., Gatehouse, P., Graves, M., Marshall, I., McRobbie, D., Papadaki, A., Semple, S., Withey, S., 2017. Specialist QC, in: McRobbie, D., Semple, S. (Eds.), IPEM Report 112: Quality Control and Artefacts in Magnetic Resonance Imaging. Institute of Physics and Engineering in Medicine, York, pp. 92–95.

Bosworth, L.A., Downes, S., 2010. Physicochemical characterisation of degrading polycaprolactone scaffolds. Polym. Degrad. Stab. 95, 2269–2276. https://doi.org/10.1016/j.polymdegradstab.2010.09.007

De Rovere, A., 2000. Characterization of hollow fiber properties during the melt spinning process.

Fan, Q., Nummenmaa, A., Wichtmann, B., Witzel, T., Mekkaoui, C., Schneider, W., Wald, L.L., Huang, S.Y., 2018. Validation of diffusion MRI estimates of compartment size and volume fraction in a biomimetic brain phantom using a human MRI scanner with 300 mT/m maximum gradient strength. Neuroimage. https://doi.org/10.1016/J.NEUROIMAGE.2018.01.004

Gates, L., Cameront, I., 1998. Time Dependent Diffusion Coefficients of Water Within Hollow Fibers. Proc. Int. Soc. Magn. Reson. Med. 1259.

Grech-Sollars, M., Hales, P.W., Miyazaki, K., Raschke, F., Rodriguez, D., Wilson, M., Gill, S.K., Banks, T., Saunders, D.E., Clayden, J.D., Gwilliam, M.N., Barrick, T.R., Morgan, P.S., Davies, N.P., Rossiter, J., Auer, D.P., Grundy, R., Leach, M.O., Howe, F.A., Peet, A.C., Clark, C.A., 2015. Multi-centre reproducibility of diffusion MRI parameters for clinical sequences in the brain. NMR Biomed. 28, 468–485. https://doi.org/10.1002/nbm.3269

Guise, C., Fernandes, M.M., Nóbrega, J.M., Pathak, S., Schneider, W., Fangueiro, R., 2016. Hollow Polypropylene Yarns as a Biomimetic Brain Phantom for the Validation of High-Definition Fiber Tractography Imaging. ACS Appl. Mater. Interfaces 8, 29960–29967. https://doi.org/10.1021/acsami.6b09809

Hubbard, P.L., Zhou, F.-L., Eichhorn, S., Parker, G.J., 2014. A crossing fibre phantom for diffusion MRI composed of co-electrospun fibres. Proc. Jt. Annu. Meet. Int. Soc. Magn. Reson. Med. – Eur. Soc. Magn. Reson. Med. Biol. 2653.

Hubbard, P.L., Zhou, F.-L.L., Eichhorn, S.J., Parker, G.J.M., 2015. Biomimetic phantom for the

validation of diffusion magnetic resonance imaging. Magn. Reson. Med. 73, 299–305. https://doi.org/10.1002/mrm.25107

Jenkinson, M., Beckmann, C.F., Behrens, T.E.J., Woolrich, M.W., Smith, S.M., 2012. FSL. Neuroimage 62, 782–90. https://doi.org/10.1016/j.neuroimage.2011.09.015

Labbaf, S., Ghanbar, H., Stride, E., Edirisinghe, M., 2014. Preparation of multilayered polymeric structures using a novel four-needle coaxial electrohydrodynamic device. Macromol. Rapid Commun. 35, 618–623. https://doi.org/10.1002/marc.201300777

Liang, C., Hu, C., Yan, K., Thomas, H., Zhu, X., 2016. Hydrophilic nonwovens by Forcespinning™ of isotactic polypropylene blended with amphiphilic surfactants. Fibers Polym. 17, 1646–1656. https://doi.org/10.1007/s12221-016-6339-5

Lucie, V., Jan, V., Karel, P., Jaroslav, B., David, L., 2014. Design of coaxial needleless electrospinning electrode with respect to the distribution of electric field. Appl. Mech. Mater. 693, 394–399. https://doi.org/10.4028/www.scientific.net/AMM.693.394

McHugh, D.J., Zhou, F., Hubbard Cristinacce, P.L., Naish, J.H., Parker, G.J.M., 2015. Ground truth for diffusion MRI in cancer: A model-based investigation of a novel tissue-mimetic material, Information Processing in Medical Imaging. https://doi.org/10.1007/978-3-319-19992-4_14

Mchugh, D.J., Zhou, F.L., Wimpenny, I., Poologasundarampillai, G., Naish, J.H., Hubbard Cristinacce, P.L., Parker, G.J.M., 2017. A biomimetic tumor tissue phantom for validating diffusion-weighted MRI measurements. Magn. Reson. Med. https://doi.org/10.1002/mrm.27016

Silva, R.A., Silva, P.A., Carvalho, M.E., 2007. Degradation studies of some polymeric biomaterials: polypropylene (PP) and polyvinylidene difluoride (PVDF). Mater. Sci. Forum 539–543, 573–576.

Teh, I., Zhou, F.-L., Hubbard Cristinacce, P.L., Parker, G.J.M., Schneider, J.E., 2016. Biomimetic phantom for cardiac diffusion MRI. J. Magn. Reson. Imaging 43, 594–600. https://doi.org/10.1002/jmri.25014

Woodruff, M.A., Hutmacher, D.W., 2010. The return of a forgotten polymer—Polycaprolactone in the 21st century. Prog. Polym. Sci. 35, 1217–1256. https://doi.org/10.1016/j.progpolymsci.2010.04.002

Yan, X., Marini, J., Mulligan, R., Deleault, A., Sharma, U., Brenner, M.P., Rutledge, G.C., Freyman, T., Pham, Q.P., 2015. Slit-surface electrospinning: A novel process developed for high-throughput fabrication of core-sheath fibers. PLoS One 10. https://doi.org/10.1371/journal.pone.0125407

Ye, A.Q., Hubbard Cristinacce, P.L., Zhou, F.-L., Yin, Z., Parker, G.J.M., Magin, R.L., 2014. Diffusion tensor MRI phantom exhibits anomalous diffusion. Conf. Proc. ... Annu. Int. Conf. IEEE Eng. Med. Biol. Soc. IEEE Eng. Med. Biol. Soc. Annu. Conf. 2014, 746–9. https://doi.org/10.1109/EMBC.2014.6943698

Zhou, F.-L., Hubbard, P.L., Eichhorn, S.J., Parker, G.J.M., 2012. Coaxially electrospun axon-

mimicking fibers for diffusion magnetic resonance imaging. ACS Appl. Mater. Interfaces 4, 6311–6. https://doi.org/10.1021/am301919s

Zhou, F.-L., Hubbard, P.L., Eichhorn, S.J., Parker, G.J.M., 2011. Jet deposition in near-field electrospinning of patterned polycaprolactone and sugar-polycaprolactone coreeshell fibres. https://doi.org/10.1016/j.polymer.2011.06.002

Zhou, F.-L., Parker, G.J.M., Eichhorn, S.J., Hubbard Cristinacce, P.L., 2015. Production and cross-sectional characterization of aligned co-electrospun hollow microfibrous bulk assemblies. Mater. Charact. 109, 25–35. https://doi.org/10.1016/j.matchar.2015.09.010

Zhou, F.L., Li, Z., Gough, J.E., Hubbard Cristinacce, P.L., Parker, G.J.M., 2018. Axon mimicking hydrophilic hollow polycaprolactone microfibres for diffusion magnetic resonance imaging. Mater. Des. 137, 394–403. https://doi.org/10.1016/j.matdes.2017.10.047